Andean growth and monsoon winds drive landscape evolution at SW margin of South America

Aurélie Coudurier-Curveur [1,2], Robin Lacassin [1] and Rolando Armijo [1]

[1] *Institut de Physique du Globe de Paris, Sorbonne Paris Cité, Univ. Paris Diderot, UMR 7154 CNRS, France.*
[2] *now at Earth Observatory of Singapore (EOS), Nanyang Technological University, Singapore.*

Lacassin@ipgp.fr (corresponding author)

ABSTRACT :

In the Atacama desert, the driest place on Earth located at the subduction margin of the Andes, the landscape evolves very slowly and changes in tectonic or erosion processes remain for a long time in the memory of topography. At latitude ~19°30'S, a threshold between exoreic and endoreic drainage regimes is clearly associated with the latitudinal gradient imposed by the modern monsoon (carrying humidity from the Atlantic) and disposed obliquely over catchments draining the Andes to the Pacific. We summarize the geomorphic, geological and climatic data in the threshold area. We then use these data to constrain numerical experiments of drainage evolution. Data and experimental results are consistent with the development of a flat low-energy morphology, close to sea level, interrupted at ≤10 Ma by tectonic uplift prevailing to the present suggesting trench-ward relief growth by incorporation of the coastal Atacama region to the Andes mountain belt.

Keywords : Andes; landscape evolution; geomorphology; orogeny; river incision; tectonic uplift

1. INTRODUCTION

The landscape at the mountain belt flanks depends to a large extent on the competing effects of tectonic uplift, which creates vertical relief, and climate, which mediates erosion (Whittaker, 2012; Bonnet and Crave, 2003). Topography, as a filtered signal of tectonics and climate (Whittaker, 2012) is a particularly important feature that keeps a record of the changes affecting these two processes. Recent studies have demonstrated that, under constant tectonics and climate, the

33   landscape retains limited information (Whittaker, 2012; Bonnet and Crave, 2003) and therefore

34   traces of past perturbations become very subtle. Long-term (>1 My) changes are commonly

35   assessed through proxies such as exhumation or sedimentary histories (e.g., for the Central Andes:

36   Schildgen *et al*., 2007; Uba *et al*., 2007). However, under the hyper-arid conditions of the Atacama

37   Desert at the west margin of the Central Andes, erosion rates are very low and time-scales of

38   landscape evolution exceed 5 My (Alpers and Brimhall, 1988; Dunai *et al*., 2005; Nishiizumi *et al*.,

39   2005; Hoke *et al*., 2007; Kober *et al*., 2007; Evenstar *et al*., 2009; Jordan *et al*., 2010). As a

40   consequence, the landscape remains transient and well-preserved long-term effects of past changes

41   of tectonic and erosion rates are still measurable in the topography.

42   The Atacama coastal morphology is marked by a conspicuous escarpment, named Coastal Scarp

43   (CS), which limits to the West the smooth upper surface of the Coastal Cordillera (CC) and a ~100

44   km-wide flat surface lying at ~1 km a.s.l. at the foot of the Andean Chain (named Pampa del

45   Tamarugal in North Chile, Figs. 1 and 2). That composite surface of Late Miocene age (eg. Farías *et*

46   *al*., 2005) may be traced almost continuously from ~16°S (South Peru) to ≥24°S (North Chile) for

47   more than 1000 km (Fig. 1a), except where locally dissected by large and deep canyons (Figs. 1a

48   and 2). In South Peru, river incision process started between 9 and 11 Ma and requires substantial

49   continuous land uplift of similar amplitude (Schildgen *et al*., 2007, 2009; Schlunegger *et al*., 2006,

50   2010). Such vertical land uplift may result from ongoing tectonic processes associated with

51   subduction (Armijo and Thiele, 1990). As in South Peru, canyon incision in North Chile is

52   relatively young (<10 My) and of comparable amplitude, implying recent tectonic uplift of ~1 km

53   (García and Herail, 2005; Zeilinger *et al*., 2005; Kober *et al*., 2006; Kirk-Lawlor *et al*., 2013). By

54   contrast, it has also been suggested that incision processes would have been triggered by climate

55   change and coastal erosion of a pre-existent topography of mid-Tertiary age (~≥25 Ma)(e.g.,

56   Mortimer and Saric, 1975; Farías *et al*., 2005; García *et al*., 2011). In that case, the kilometric

57   coastal uplift would be much older than the incision processes.

58

59   In order to discuss the incision mechanism in North Chile, we focus our study on a threshold area

60   where, over a distance of less than 100 km, the drainage system changes from clearly exoreic

61   (northernmost Chile, 18°30'S) to clearly endoreic South of 19°35'S (e.g., Hoke *et al*., 2007; García

62   *et al*., 2011) (Figs. 1 & 2). First, we review the geology and geomorphology of the threshold area.

63 Then, we identify and characterize key measurable elements of the landscape. We note that current

64 meteorological data (Strecker *et al.*, 2007; Bookhagen and Strecker, 2008) indicate that the

65 latitudinal rainfall gradient, which is imposed by the modern monsoon, crosses obliquely the

66 Altiplano (AP) and the Western Cordillera (WC) (Fig. 1b) and appears to control spatial variations

67 of drainage erosion power in the threshold area. Finally, using a numerical modeling, we explore a

68 set of scenarios adopting two simple conditions: (1) the topographic relief in the threshold area has

69 experienced uniform tectonic uplift during the past 10 Ma, and (2) the actualistic hypothesis that the

70 present-day pattern of the monsoon regime can help us to explain the long-term development of

71 drainage in the threshold area.

72

73 **2. GEOLOGIC, GEOMORPHIC AND CLIMATIC FRAMEWORK**

74

75 **2.1 *Basic geology and geomorphology***

76 The flat surface of the Pampa del Tamarugal corresponds to the western part of an extensive erosion

77 surface, called Atacama Pediplain (e.g., Hartley and Evenstar, 2010), which marks the top of the

78 continental wedge-shaped Central Depression Basin (CDB), formed between ~30 and ~10 Ma as a

79 foreland basin over the west piedmont of the growing Andes (Hartley and Evenstar, 2010;

80 Schlunegger *et al.*, 2010) (discussing the evolution of the CDB is beyond the scope of this paper

81 however, we present a schematic evolution in Fig.7). Broad features of the geology of the Andean

82 subduction margin, including the CC, CDB, and Pampa del Tamarugal, follow the geometry of

83 Andean structures, and appear thus controlled by large-scale faults at major boundaries, i.e., the

84 subduction plate contact (Armijo & Thiele, 1990) and the West Andean Thrust (WAT, Fig. 1c;

85 Armijo *et al.*, 2010, Armijo *et al.*, submitted). In South Peru, the CDB preserves an intercalated

86 marine sediment layer of 25 Ma old (Thouret *et al.*, 2007), which is now found at ~2000 m

87 elevation (Thouret *et al.*, 2007; Schildgen *et al.*, 2009). At that time, sedimentation in the Andes

88 piedmont was occurring close to sea level. Later, the whole sedimentary sequence of the CDB was

89 uplifted and incised by deep canyons grading to the oceanic base level from headwaters located in

90 the WC and AP (Fig. 1). Thermochronology data and $^{40}Ar/^{39}Ar$ age determinations (Thouret *et al.*,

91 2007; Schildgen *et al.*, 2009; Schildgen *et al.*, 2010) imply canyon incision after ~9 Ma requiring

92 kilometric differential uplift of the WC with respect to its piedmont and ~1 km of overall land uplift

93   of the whole coastal block (from the coast to the AP) with respect to the oceanic base-level

94   (Schildgen *et al*., 2009).

95   In northernmost Chile, similar canyons have been carved into the whole margin, between the AP

96   and the Pacific. The incision amplitude reaches 1 km deep across the CC and sediments of the

97   CDB. There the top of the CBD corresponds to the Miocene El Diablo formation (Charrier *et al*.,

98   2007), likely deposited in a braided plain linking the CDB with the Pacific Ocean (Schlunegger *et*

99   *al*., 2010) and now found at elevation of ~0.6-1 km close to the coast. The topmost layers of the El

100   Diablo formation are ~8-10 Ma old (Naranjo and Paskoff, 1985; von Rotz *et al*., 2005; Schlunegger

101   *et al*., 2010). The maximum onset time of canyon incision is therefore younger than ~10 Ma (García

102   and Hérail, 2005; Schlunegger *et al*., 2006; Schlunegger *et al*., 2010; García *et al*., 2011). This

103   process appears associated with the presence of the 1-km-high Coastal Scarp (Figs. 1, 2, 4; Armijo

104   and Thiele, 1990) as well as with the occurence of large active normal faulting parallel to that scarp

105   (such as the Pisagua Fault, Fig. 4a). This suggests that, similar to South Peru, significant protracted

106   land uplift relative to the oceanic base level has occurred in North Chile over less than 10 Ma

107   (Armijo and Thiele, 1990; Armijo *et al*., submitted).

108   ***2.2 Main features of Tiliviche threshold***.

109   At 19°35'S, the threshold between exoreic and endoreic drainage (Fig. 2) is accurately defined by

110   using the Tana-Tiliviche river catchment as a reference (Figs. 2, 3b and 4a). The lower course of

111   Tiliviche has a convex upward longitudinal profile and a prominent knick-zone at a distance of ~25

112   km from the CS (Figs. 3b, 4a). There, the stream channel is deeply incised below the Atacama

113   pediplain surface (≥800m, Fig. 5b). A dated strath terrace perched at ~50 m below the top of the

114   canyon (Figs. 4a, 5b) located ~15 km from the CS (6.4 Ma, Hoke *et al*., 2007), suggests that the

115   river was already crossing the CC, reaching the ocean base level before its main incision (Kirk-

116   Lawlor *et al*., 2013). East of the knick zone (Figs. 4a, 5b), this deep canyon becomes almost

117   superficial (< 200 m deep) across the CDB and is limited in its connection with the well-developed

118   upper drainage incising the WC. Rivers to the north of Tiliviche (typified by Camarones, Figs. 2,

119   5a) are all deeply entrenched from the CS to the WC and show concave longitudinal profiles

120   (Fig. 3a, 5a) for distances of ≥ 50 km from the CS. South of Tiliviche, the upper rivers incising the

121   WC discharge and aggrade in the Pampa del Tamarugal at ~1 km a.s.l., while a few minor streams

122   drain across the CS to the Pacific (Figs. 2, 3c, 5c). Profiles of those upper drainages reveal several

123   knick-points (Fig. 3c), which are considered to result from differential uplift of the WC relative to

124   the Pampa del Tamarugal surface (Hoke *et al.*, 2007). The only exception to endoreism between

125   19°35'S and 23°S concerns the Loa river (Fig. 2). Its source is located behind the WC topographic

126   relief, on the Altiplano plateau, with a catchment area much larger than those of endoreic rivers,

127   implying larger water supply and therefore a more efficient erosional power. For further discussion

128   and modeling purposes, we select the three stream profiles typifying the threshold: Camarones,

129   Tiliviche and Tarapacá (Figs. 3 & 5).

130   For several tens of km North and South of the Tiliviche canyon, the CC is a smooth, relictual relief,

131   which evolved for a long time under extremely low erosion rates (Kober *et al.,* 2007), and have

132   little elevation difference relative to the Pampa del Tamarugal surface (Fig. 4). That low-energy

133   relief is now dramatically rejuvenated by the 1-km-high CS and deep canyon incisions (Figs. 4, 5).

134   We note that the Atacama Pediplain and the CS keep uniform morphology and elevation throughout

135   the threshold area and that all streams are now incised across the same morphologic and geological

136   units (CC, CDB) trending roughly North-South. We infer therefore that differences of stream

137   morphology are not associated with latitudinal variations of uplift rate or of rock erodibility, but

138   more likely to latitudinal variation of river erosional power, which we select as a critical factor for

139   modeling.

140   ***2.3 Oblique rainfall gradient over the South Central Andes: hyper-aridity of the Atacama region***

141   Erosion, and by extension precipitation rates, in the Atacama Desert significantly declined after 15

142   Ma (e.g., Alpers and Brimhall, 1988; Sillitoe and McKee, 1996), which corresponds to a major

143   global cooling event (see discussion by Gregory-Wodzicki, 2000) and correlates stratigraphically

144   with the end of significant sediment deposition in the CDB and with completion of the Atacama

145   pediplain. Together with other evidence of long-lived aridity in the Atacama Desert (Houston and

146   Hartley, 2003; Dunai *et al.*, 2005; Hartley and Chong, 2005; Evenstar *et al.*, 2009) this implies a

147   relatively uniform evolution towards hyper-aridity, clearly established since ~15 Ma.

148   In the present day, moisture is mostly brought toward the WC and Atacama Desert by northeasterly

149   monsoonal airflow (Houston and Hartley, 2003; Strecker *et al.*, 2007; Garreaud, 2009). The

150   considerable distance from both Atlantic and Amazonian sources of humidity to the western Andean

151   margin is the first cause of hyper-aridity in the Atacama. Other factors, such as the cold Humboldt

152   oceanic current, also contribute to hyperaridity by preventing inland penetration of moisture coming

153 from the Pacific (Houston and Hartley, 2003; Garreaud, 2009). As a consequence, present-day

154 precipitation decreases southwestward across the AP, causing isohyets to be oblique to the Andean

155 relief south of 15°S (Houston and Hartley, 2003; Bookhagen and Strecker *et al*., 2008; Garreaud,

156 2009) and producing the latitudinal rainfall gradient over the western AP and WC clearly visible in

157 maps (Figs. 1, 6). In South Peru, the gradient is parallel to the coast and the WC and headwaters of

158 catchments draining to the Pacific experience precipitation rates ≥200 mm/yr (Fig. 6). In North

159 Chile, mean annual rainfall on the WC decreases southward to ≤50 mm/yr south of ~20°S (Fig. 6).

160 In both South Peru and North Chile, rainfall is almost null on the Pampa del Tamarugal and towards

161 the coast (≤5 mm/yr of precipitation). Regarding our actualistic modeling approach, we retain the

162 observed oblique spatial pattern of present-day rainfall in the WC, upstream from the three

163 catchments typifying the Tiliviche threshold. In other words, our approach assumes and tests

164 stability over the long term of oblique monsoonal conditions across the WC, which is consistent

165 with long-lived hyper-aridity in the Atacama Desert and with evidence for monsoonal conditions in

166 the eastern Andes, on the landward side of the Altiplano, since ~≥10 Ma (Uba *et al*., 2007; Mulch *et*

167 *al*., 2010).

168 *2.4 North Chile canyon incision: climatic or tectonic driver ?*

169 In contrast with the evidence summarized above and the doubtless recent uplift of coastal South

170 Peru (Schildgen *et al*., 2007, 2009), it has for long been considered that uplift of coastal regions in

171 North Chile would be much older than the ~<10 Ma incision of canyons (e.g., Mortimer and Saric,

172 1975; Farías *et al*., 2005; García *et al*., 2011). It has been suggested that the top surface of the CDB

173 was dammed by pre-existing CC reliefs and stood for a long time as an elevated base level not

174 connected to the ocean (e.g., Mortimer and Saric, 1975; García *et al*., 2011). Canyon incision, and

175 eventual connection of the drainage to the ocean, would have been recently triggered by runoff

176 increases associated with hypothetic semi-arid pulses interrupting the prevalent hyper-arid regime

177 (García *et al*., 2011). This transition to exoreic drainage would have been more efficient and rapid

178 in the North because of the latitudinal rainfall gradient (García *et al*., 2011). These authors also

179 consider that incision processes would not have been synchronous along the margin. There is no

180 compelling geological evidence for such a complex scenario and the notion of old uplift (~≥25 Ma)

181 with uncorrelated incision appears controversial (e.g. Zeilinger *et al*., 2005; Kober *et al*., 2006;

182 Schildgen *et al*., 2007; Schlunegger *et al*., 2006, 2010; Hoke *et al*., 2007; Jordan *et al*., 2010; Kirk-

183   Lawlor *et al*., 2013). So here, we choose to retain the simplest hypothesis of relatively stable hyper-

184   aridity since ~15 Ma, and to test the idea that the flat, western part of the Atacama Pediplain was

185   initially forming an Andean piedmont close to the ocean base-level (Fig.7), and that overall uplift of

186   this piedmont relative to the ocean triggered the headwards incision of canyons since ~<10Ma

187   (García and Hérail, 2005; Schildgen *et al*., 2007; Schlunegger *et al*., 2006, 2010; Kirk-Lawlor *et al*.,

188   2013).

189

190   **3. MODELING OF DRAINAGE EVOLUTION**

191   **3.1 *Modeling strategy***

192   From the descriptions and discussion detailed in Part 2, we retain several relevant statements for our

193   modeling of drainage in North Chile: (1) the uplift of the Andean piedmont starts at ~10 Ma or even

194   younger and triggered headwards incision of rivers (Fig.7) as demonstrated for canyons in South

195   Peru; (2) the first-order geomorphic and geological continuity of coastal units throughout the

196   identified drainage threshold implies that differences of stream morphology are likely associated

197   with latitudinal variation of river erosional power; (3) the threshold between exoreic and endoreic

198   drainage regimes is correlated with the latitudinal gradient imposed by the modern monsoon

199   (carrying humidity from the Atlantic); (4) the hyper-aridity on coastal North Chile and the present-

200   day oblique monsoonal conditions across the WC are stable features on the long-term. We use these

201   inferences to settle a numerical model of landscape evolution using the code of [Carretier and

202   Lucazeau, 2005].

203   **3.2 *The numerical landscape model APERO***

204   As with other landscape evolution models (e.g. SIBERIA (Willgoose *et al*., 1991), CAESAR

205   (Coulthard *et al*., 2002) GOLEM (Tucker and Slingerland, 1994), CASCADE (Braun & Sambridge,

206   1997), CHILD (Tucker & Bras, 2000), EROS (Davy and Crave, 2000)), the APERO code models

207   landscape evolution by routing water and sediments over a grid of regular cells, starting from cells

208   at the highest elevation and moving progressively to the lowest ones. It calculates elevation changes

209   according to sediment production resulting from diffusion, alluvial transport and bedrock incision.

210   The principles of APERO (Carretier, 2002; Carretier & Lucazeau, 2005) are described here in

211   simple terms and in more detail in the Supplementary Information.

212

213   The governing equations used in APERO are the conservation equations of mass for water (Eq.1)

214   and for sediments (Eq.2) that are separately numerically solved with the finite difference method.

215
$$\frac{\partial h_f}{\partial t} - Q_{f\,IN} + Q_{f\,OUT} = 0 \qquad\qquad (Eq.1)$$

216   with h_f the water thickness integrated over the cell size, $Q_{f\,IN}$ the input water flux and $Q_{f\,OUT}$ the

217   output water flux.

218
$$\frac{\partial h_s}{\partial t} - Q_{s\,IN} + Q_{s\,OUT} + U = 0 \qquad\qquad (Eq.2)$$

219   with h_s the ground elevation integrated over the cell size, $Q_{s\,IN}$ the input sediment flux, $Q_{s\,OUT}$ the

220   output sediment flux and U, the tectonic uplift rate integrated over the cell size. In Eq.1 and Eq.2,

221   the fluxes and the uplift rate have dimensions of $[L^3\,T^{-1}]$.

222    $Q_{f\,IN}$ scales with the effective mean precipitation rate within the catchment relative to the cell (i),

223   including the cell (i) itself.

224
$$Q_{f\,IN\,(i)} = \int_A P_d\,(x,y)\,ds \qquad\qquad (Eq.3)$$

225   P_d is the effective mean precipitation rate $[LT^{-1}]$ and A is the catchment area relative to cell i.

226   Each cell (i) interacts with its neighboring cells (j) depending on the difference in topography

227   between the two cells. We define $S_{ij} = \max(0, (h_i - h_j)/d_{ij})$ where d_{ij} is the distance between the

228   two cells. The distribution of water from cell i to cell j ($Q_{f\,OUT\,(ij)}$) follows Eq.4, called multiple flow

229   algorithm:

230
$$Q_{f\,OUT\,(ij)} = Q_{f\,IN\,(i)}\,\frac{S_{ij}}{\sum_j S_{ij}} \qquad\qquad (Eq.4)$$

231   The total output flux $Q_{f\,OUT(i)}$ is the sum over (j) of the local $Q_{f\,OUT\,(ij)}$.

232   The input sediment flux $Q_{s\,IN(i)}$ on a cell i is the sum of the local outputs $Q_{s\,OUT\,(ij)}$ of sediments

233   from the upper cells which are distributed according to the following algorithm.

234   The output sediment flux $Q_{s\ OUT\ (i)}$ on a cell (i) (Eq.5) corresponds to the joint action of diffusion

235   processes (Eq.6 and Eq.7), alluvial transport (Eq.8) and bedrock incision processes (Eq.9) occurring

236   on a cell,

237                       $$Q_{s\ OUT} = Q_{snldiff} + Q_{sal} + Q_{br} \qquad\qquad \text{(Eq.5)}$$

238   The component of sediment output due to bedrock diffusion processes, $Q_{snldiff}$ or diffusive

239   transport rate (Eq.6), is written as a non-linear diffusion equation (Roering *et al.*, 1999) (Eq.7) to

240   take into account landslide processes where:

241                       $$Q_{snldiff} = \nabla . q_{snldiff} \qquad\qquad \text{(Eq.6)}$$

242                       $$q_{snldiff} = -\kappa \ \frac{\nabla h_s}{1-(\frac{\nabla h_s}{S_c})^2} \qquad\qquad \text{(Eq.7)}$$

243   with S_c the critical slope corresponding to the gradient of repose of sediments or bedrock and κ a

244   diffusion coefficient $[L^2\ T^{-1}]$. Note that κ depends on rock type (either sediment, or bedrock or a

245   combination of the two, see Supplementary Information).

246   The alluvial transport flux, Q_{sal}, and the bedrock incision flux integrated over the river width, Q_{br},

247   are written as power-law equations:

248                       $$Q_{sal} = K_{al}\ Q_{f\ OUT}{}^{\alpha}\ S_{ij}{}^{\beta} \qquad\qquad \text{(Eq.8)}$$

249                       $$Q_{br} = K_{br}\ Q_{f\ OUT}{}^{m}S_{ij}{}^{n} \qquad\qquad \text{(Eq.9)}$$

250   where K_{al} and K_{br} are positive coefficients with dimensions $[L^{3-3\alpha}\ T^{\alpha-1}]$ and $[L^{3-3m}\ T^{m-1}]$. α,

251   β, m and n determine the degree of non-linearity of the two laws and m and n have values

252   comprised between 0 and 2 (Stock & Montgomery, 1999).

253   Further details on the numerical implementation and on model calibration (grid size,

254   characterization of K_{al} α, β, K_{br}, m and n, choice of parameters values, etc.) are given in the

255   Supplementary Information (SI) with pertinent references herein.

256   **3.3 *Model Setting***

257   We ran numerical experiments of landscape evolution using the modeling code of [Carretier and

258   Lucazeau, 2005]. The experimental grid is scaled to reproduce the topography of the threshold area

259   of North Chile and to reach the present-day stage after 7 My of evolution: the minimum likely age

260   for North Chile onset time of incision. Experiments start with an initially flat, low-energy coastal

261   topography that lies at sea level. The WC-AP is a pre-existing relief (Victor *et al*., 2004; Hoke *et al*.,

262   2007; Jordan *et al*., 2010).   In agreement with the geological constraints, a value of 0.14 mm/yr is

263   used for the uplift rate at the coast rising to 0.22 mm/yr at the WC (see supplementary information

264   for a detailed discussion). Those rates remain constant during the experiment. The final modeled

265   topography compares well with the current one, including the formation of a 1-km-high CS (Figs. 7,

266   S1). Rainfall is null at the coast and on the Pampa del Tamarugal surface and is mostly localized

267   above the upper WC and AP reliefs (Fig. S1). Several values of precipitation rates were tested (from

268   20 to 200 mm/yr on the WC) to take into account the possible effect of the latitudinal rainfall

269   gradient. Infiltration and evaporation cannot be addressed by our modeling, so water flows at the

270   surface and goes out from the model grid at its left (West) boundary (Carretier and Lucazeau, 2005).

271   Refer to Supplementary Information (SI) (Table S1 and Figures S2 to S9) for a complete summary

272   of other boundary conditions. Parameters controlling the physics of the erosion processes are fixed

273   according to published values (references given in SI), or chosen among values producing the

274   observed morphology, after sensitivity analyses (see SI Part C, Table S2 and Figures S2 to S9).

275

276   ***4. EXPERIMENTAL MODELING RESULTS, LIMITATIONS AND IMPLICATION***

277

278   **4.1 Topography and river drainage evolution: model vs. natural landscape**

279   We simulate the evolution of river incision onto an uplifting coastal block under three different

280   constant rainfall conditions (low, intermediate and high Precipitation Rates) during 7 My in

281   agreement with the present-day precipitation rates (PR) distribution over North Chile. Figure 8b

282   shows the modeling results of the three corresponding experiments where river long profiles can be

283   compared to the three stream profiles typifying the threshold in North Chile: Camarones, Tiliviche

284   and Tarapacá. In the experiments, dendritic drainage catchments form as the coastal topography

285   rises without being significantly eroded, except where river incision develops.

286   For the higher values of PR (Fig. 8b-top), the main streams are deeply incised in the coastal

287   topography and grade to the oceanic base level. The river profile is nearly in equilibrium for ~80

288   km from the coast up to the WC. This result is comparable to the Camarones river profile that is

289 uniformly deeply entrenched in the topography from the Altiplano plateau towards the oceanic base

290 level. Water supply appears therefore to be sufficient to allow a full river incision from high

291 elevations (4000 m) to the oceanic base level.

292 For the intermediate PR values (Fig. 8b-middle), the stream presents a concave shape; lower and

293 upper stream courses are nearly separated, with little incision in the middle course and a knick-point

294 forms at ~40 km from the coast. This concave shape means that the stream is not in equilibrium,

295 contrary to the first experiment with higher value of PR. The profile is comparable to the Tiliviche

296 river profile whose incision is five times lower in the middle of the coastal plateau than it is closer

297 to the Coastal Scarp. This implies that water supply is not high enough to enable a spatially constant

298 incision into the uplifting topography.

299 For the lower PR values (Fig. 8b-bottom), incision in the middle course of streams is replaced by

300 aggradation on top of the rising coastal topography. The water flows at the surface and drives

301 incision of the lower course and formation of a knick-point at ~20 km from the coast. This

302 numerical experiment result can be compared to the Tarapacá river incision. The stream incises only

303 the upper part of the topography, does not entrench the coastal plateau and consequently does not

304 reach the oceanic base level.

305

306 **4.2 Limitations and drawbacks**

307 We acknowledge that our experiments are simple first-order ones and do not take into account

308 several natural processes occurring in North Chile that may play a role on the final results.

309 However, we note that our results compare qualitatively well with the observed landscape

310 morphology and its variability. Yet, our modeling approach has some limitations that we discuss

311 here before further exploring the implications of the results.

312 First, the model involves 12 parameters for most of which there is no direct natural geological or

313 hydrological quantitative constraints. So, it has been necessary to (1) determine the dominant

314 parameter for our modeling and investigate the effects of its possible values and (2) calibrate each

315 parameter with tests within ranges of published values. Because there is little sediment cover on the

316 riverbed in North Chile, the evolution of topography is likely governed by detachment-limited

317 process justifying the choice of the bedrock incision parameter (K_{br}) as one of the main controls in

318 our modeling. As there is no specific constraint for this parameter respective to North Chile rivers,

319 we tested several values published in the literature and considered two end-members values along

320 with an intermediate one. We ran a sensitivity analysis for each of the other parameters and

321 calibrated the model with their most pertinent value (cf. SI). We present here our preferred solution

322 and we acknowledge that this is not a unique solution.

323 Second, while most authors regroup rock erodibility and climatic effects into the bedrock incision

324 parameter, an assumption that is correct for steady-state systems, we note that, in a transitory

325 regime, PR also acts in the alluvial transport process (Eq.8). This justifies our choice to use distinct

326 K_{br} and PR. Our results imply that, for a given value of K_{br}, the threshold between exoreic and

327 endoreic drainage systems is controlled by differences in PR. However, comparable result could

328 have been obtained for other combinations of K_{br} and PR. Increasing erodibility balances with

329 decreasing PR, and inversely (Eq.9). Our sensitivity analysis highlights this trade-off between

330 erodibility and PR (see Fig.S5 to S9).

331 Third, we use mean annual PR values derived from present day precipitation rates measured over a

332 9 years period (1998 to 2006) (data from [Bookhagen *et al*., 2008]). Extrapolating those present-day

333 rates over a 7 My-time scale is justified by studies of erosion, mineralization and soil development

334 carried out in the Atacama Desert that show that PR have been lower than 200 mm/yr over the last

335 20 My (Alpers and Brimhall, 1988; Rech *et al*., 2006). However, rainfall in the Atacama Desert area

336 occurs as infrequent distinct events of relatively large amplitude and not as continuous rainfall.

337 Bedrock incision due to such discrete events is likely higher than the incision resulting from a

338 constant mean rainfall. We used a 10-years time step in the modeling that simulates to a certain

339 degree this kind of discrete rainfall event. However, the influence of short-term (10-100 years)

340 variability of PR on the evolution of the landscape will have to be more carefully investigated for

341 further quantitative studies.

342 Other limitations come from the fact that our modeling does not allow for evaporation of

343 infiltration. In North Chile (Fig. 8a middle and bottom), part of the water flow leaks or evaporates

344 while crossing the Pampa del Tamarugal, resulting in less incised lower streams than in the

345 experiments, and knick-points closer to the coast. Another difference is that the experimental upper

346 course of catchments is also more entrenched into the WC topographic relief than in nature

347 (compare natural and experimental river profiles on Fig. 8). It is probable that part of the

348 precipitation occurring over the west AP and WC does not contribute to the surface flow and instead

349 infiltrates the bedrock causing springs to form at lower elevation on the flanks of the WC as

350 described by [Hoke *et al*., 2004]. Also, a thick resistant flows of Miocene ignimbrite covers the WC

351 topography and may prevent efficient erosion. In our experiments, we used a uniform bedrock

352 incision parameter over the entire box, but the effect of this ignimbritic cover may be assessed

353 looking at the sensitivity analyses for different values of K_{br}.

354 Time scaling is difficult to test with our experiments. We must acknowledge that we adjusted the

355 modeling parameter values to allow for drainage development over a 7 My-time scale, which is

356 deduced from geological observations for the onset of incision (eg. Naranjo and Paskoff, 1985;

357 Hoke *et al*., 2004). With this taken into account, we note that with constant uplift rate and different

358 values for PR, our model, run for 7 My, is able to reproduce the different drainage systems we

359 identified in the threshold area.

360

361 **4.3 Climatic and geodynamic implications**

362 From the comparison of experimental and natural drainages (Fig. 8), we deduce that retaining

363 experimental PR values in the range of present-day values is enough to explain the development of

364 that drainage, including its latitudinal variation and specifically the occurrence of the Tiliviche

365 threshold. More specifically, under constant tectonic uplift, the occurrence of that threshold requires

366 a stable latitudinal gradient of precipitation over the WC, similar to the modern one. We note that

367 the condition of keeping such stable latitudinal PR gradient needs to take into the account the trade-

368 offs between the different modeling parameters and in particular the one between basement

369 erodibility and precipitation rate. This implies a set of possible stable solutions consistent with

370 monsoon regimes with different precipitation intensity (within a range of PR values), but

371 maintaining stable spatial extent and latitudinal gradient over the WC.

372 Both geological observations and model support the idea of a flat low-energy coastal morphology

373 located close to the Pacific Ocean base level as initial conditions prior to ca. 7 Ma. As there may be

374 a lag time between uplift and related incision processes, we consider the age of 7 Ma as a minimum

375 age for the onset of uplift, which could be a few millions years older. So, at ~10 Ma, in North Chile

376 and South Peru, the southwestern Andean piedmont had probably begun to experience synchronous

377 and uniform uplift triggered by a dramatic tectonic change. The uplift added ~1 km of elevation to

378 the onshore Andean subduction margin limited to the West by the Coastal Scarp (Fig. 1c). This

379   recent uplift of the coastal topography implies to consider a trench-ward enlargement of the Andean

380   topographic relief by incorporation of the coastal Atacama region to the Andes-Altiplano orogen

381   (Armijo *et al.*, submitted). Deep crustal underplating, probably associated with fault geometrical

382   complexities at the subduction plate interface and above (Armijo and Thiele, 1990; Contreras-Reyes

383   et al., 2012), is a possible cause of coastal uplift and widening of the Andean orogen (Armijo *et al.*,

384   submitted). Structural complexities may also control segmentation of the mechanically coupled

385   zone at the subduction interface, as recently suggested by [Béjar-Pizarro et al., 2013]. So, recent

386   (<10 Ma) Andean deformation is not only located on the eastern side of the orogen as generally

387   admitted (eg. McQuarrie *et al.*, 2004; Oncken *et al.*, 2006) but also proceeds by widening of the belt

388   towards the subduction, which brings new insights into the process of propagation of the

389   deformation across the entire mountain range.

390

5. CONCLUSIONS

392   Numerical modeling of landscape evolution in North Chile allowed us to test the hypothesis of

393   recent uniform tectonic uplift driving river incision in the past 10 My over the west Andean margin.

394   Our results offer a simple framework with a reduced number of semi-quantitative geomorphic

395   parameters, which we used to explain the modern evolution of both, morphology and tectonics, as

396   deciphered from their quantitative imprint in the present-day landscape. An important result is that

397   the latitudinal transition from exoreic to endoreic drainage systems across the Atacama Desert of

398   North Chile would be primarily controlled by a spatial gradient of precipitation rates over the

399   headwaters of rivers in the Western Cordillera. Gradient patterns required in our modeling are

400   similar to present-day conditions of precipitation rates; a result suggesting that the rainfall patterns

401   in the Western Cordillera and the Atacama Desert, largely controlled by the effect of Atlantic

402   monsoon, are long-lived features of Andean climate.

403

404

409   on the experimental approach. We thank anonymous reviewers and the editor for their very helpful

410   and constructive comments.

411

412

413

414   **REFERENCES**

415

416   Alpers, C. N., and G. H. Brimhall, 1988, Middle Miocene climatic-change in the Atacama Desert,

417   northern Chile - evidence from supergene mineralization at La Escondida, Geol. Soc. Am. Bull.,

418   100(10), 1640-1656, doi: 10.1130/0016-7606(1988)100<1640:mmccit>2.3.co;2.

419   Armijo, R., and Thiele, R., 1990, Active faulting in northern Chile: ramp stacking and lateral

420   decoupling along a subduction plate boundary?: Earth and Planetary Science Letters, v. 98, no. 1, p.

421   40–61, doi: 10.1016/0012-821X(90)90087-E.

422   Armijo, R., Rauld, R., Thiele, R., Vargas, G., and Campos, J., Lacassin, R., and Kausel, E., 2010,

423   The West Andean Thrust, the San Ramón Fault, and the seismic hazard for Santiago, Chile:

424   Tectonics, v. 29, TC2007, doi: 10.1029/2008TC002427.

425   Armijo, R., Lacassin, R., Coudurier-Curveur, A. and Carrizo, D., 2014, Coupled tectonic evolution

426   of Andean orogeny and global climate, Tectonics, *submitted*.

427   Béjar-Pizarro, M., Socquet, A., Armijo, R., Carrizo, D., Genrich, J., and Simons, M., 2013, Andean

428   structural control on interseismic coupling in the North Chile subduction zone, Nature Geoscience,

429   v. 6, p. 462-467, doi: 10.1038/NGEO1802.

430   Bonnet, S., and Crave, A., 2003, Landscape response to climate change: Insights from experimental

431   modeling and implications for tectonic versus climatic uplift of topography: Geology, v. 31, no. 2,

432   p. 123–126, doi: 10.1130/0091-7613(2003)031<0123:LRTCCI>2.0.CO;2.

433   Bookhagen, B., and Strecker, M.R., 2008, Orographic barriers, high resolution TRMM rainfall,

434   and relief variations along the eastern Andes: Geophysical Research Letters, v. 35, no. 6, L06403,

435   doi: 10.1029/2007GL032011.

436   Braun, J. and Sambridge, M., 1997, Modelling landscape evolution on geological time scales: a new

437   method based on irregular spatial discretization, Basin Research, 9: 27-52

Carretier, S. and Lucazeau, F., 2005, How does alluvial sedimentation at range fronts modify the erosional dynamics of mountain catchments ?: Basin Research, v. 17, p. 361–381, doi: 10.1111/j.1365-2117.2005.00270.x

Charrier, R., Pinto, L., and Rodríguez, M. P., 2007, Tectonostatigraphic evolution of the Andean Orogen in Chile, in The Geology of Chile, edited by T. Moreno and W. Gibbons, pp. 21–114, The Geological Society, London.

Contreras-Reyes, E., Jara, J., Grevemeyer, I. , Ruiz, S., and Carrizo, D., 2012, Abrupt change in the dip of the subducting plate beneath north Chile, Nature Geoscience, 5, 342–345, doi: 10.1038/ngeo1447.

Coulthard, T.J., Macklin, M.G. and Kirkby, M.J., 2002, A cellular model of Holocene upland river basin and alluvial fan evolution, Earth Surface Processes and Landforms, v.27, n.3, p, 269-288

Davy, P., and Crave, A., 2000, Upscaling local-scale transport processes in large-scale relief dynamics, Physics and Chemistry of the Earth, Part A: Solid Earth and Geodesy, 25(6–7), 533-541, doi:10.1016/S1464-1895(00)00082-X.

Dunai, T.J., González López, G.A., and Juez-Larré, J., 2005, Oligocene–Miocene age of aridity in the Atacama Desert revealed by exposure dating of erosion-sensitive landforms: Geology, v. 33, p. 321-324, doi: 10.1130/G21184.1.

Evenstar, L., Hartley, A., Stuart, F., Mather, A., Rice, C., and Chong, G., 2009, Multiphase development of the Atacama Planation Surface recorded by cosmogenic [3]He exposure ages: Implications for uplift and Cenozoic climate change in western South America: Geology, v. 37, p. 27-30, doi: 10.1130/G25437A.1.

Farías, M., R. Charrier, D. Comte, J. Martinod, and G. Hérail, 2005, Late Cenozoic deformation and uplift of the western flank of the Altiplano: Evidence from the depositional, tectonic, and geomorphologic evolution and shallow seismic activity (northern Chile at 19°30'S), Tectonics, 24, TC4001, doi:4010.1029/2004TC001667.

García, M., and G. Hérail, 2005, Fault-related folding, drainage network evolution and valley incision during the Neogene in the Andean Precordillera of Northern Chile, Geomorphology, 65, 279-300.

García, M., Riquelme, R., Farías, M., Hérail, G., and Charrier, R., 2011, Late Miocene-Holocene canyon incision in the western Altiplano, northern Chile: tectonic or climatic forcing?: Journal of the Geological Society, v. 168, p. 1047–1060, doi: 10.1144/0016-76492010-134.

Garreaud, R.D., 2009, The Andes climate and weather: Advances in Geosciences, v. 22, p. 3–11, doi: 10.5194/adgeo-22-3-2009.

Gregory-Wodzicki, K. M., 2000, Uplift history of the Central and Northern Andes: A review, Geological Society of America Bulletin, 112(7), 1091-1105, doi: 10.1130/0016-7606(2000)112<1091:uhotca>2.3.co;2.

Hartley, A.J., Chong, G., Houston, J., and Mather, A.E., 2005, 150 million years of climatic stability: evidence from the Atacama Desert, northern Chile: Journal of the Geological Society, v. 162, p. 421–424, doi: 10.1144/0016-764904-071.

Hartley, A.J., and Evenstar, L., 2010, Cenozoic stratigraphic development in the north Chilean forearc: Implications for basin development and uplift history of the Central Andean margin: Tectonophysics, v. 495, p. 67-77, doi: 10.1016/j.tecto.2009.05.013.

Hoke, G.D., Isacks, B.L., Jordan, T.E. and Yu, J.S., 2004, Groundwater sapping origin for the giant quebradas of northern Chile, Geology, v. 32 (7), p. 605-608

Hoke, G.D., Isacks, B.L., Jordan, T.E., Blanco, N., Tomlinson, A.J., and Ramezani, J., 2007, Geomorphic evidence for post-10 Ma uplift of the western flank of the central Andes 18°302–22°S: Tectonics, v. 26, p. 17, doi: 10.1029/2006TC002082.

Houston, J., and Hartley, A.J., 2003, The central Andean west-slope rainshadow and its potential contribution to the origin of hyper-aridity in the Atacama Desert: International Journal of Climatology, v. 23, p. 1453–1464, doi: 10.1002/joc.938.

Jordan, T. E., P. L. Nester, N. Blanco, G. D. Hoke, F. Dávila, and A. J. Tomlinson, 2010, Uplift of the Altiplano-Puna plateau: A view from the west, Tectonics, 29, TC5007, doi: 10.1029/2010TC002661.

Kirk-Lawlor, N. Jordan, T.E., Rech, J.A., and Lehmann, S., 2013, Late Miocene to Early Pliocene paleohydrology and landscape evolution of Northern Chile, 19° to 20°S, Palaeogeography, Palaeoclimatology, Palaeoecology, 387: 76-90

Kober, F., Schlunegger, F., Zeilinger, G., and Scheider, H., 2006, Surface uplift and climate change : The geomorphic evolution of the Western Escarpment of the Andes of northern Chile between the Miocene and present: GSA Special Papers 2006, v. 398, p.75-86, doi: 10.1130/2006.2398(05).

Kober, F., Ivy-Ochs, S., Schlunegger, F., Baur, H., Kubik, P., and Wieler, R., 2007, Denudation rates and a topography-driven rainfall threshold in northern Chile: Multiple cosmogenic nuclide data and sediment yield budgets: Geomorphology, v. 83, p. 97–120, doi: 10.1016/j.geomorph.2006.06.029.

McQuarrie, N., 2002, The kinematic history of the central Andean fold-thrust belt, Bolivia: Implications for building a high plateau, GSA Bulletin, v. 114(8), p. 950-963

Mortimer, C., and Saric, R. N., 1975, Cenozoic studies in northernmost Chile: Geologische Rundschau, 64, 395-420.

Mulch, A., Uba, C.E., Strecker, M.R., Schoenberg, R., and Chamberlain, C.P., 2010, Late Miocene climate variability and surface elevation in the central Andes: Earth and Planetary Science Letters, v. 290, p. 173–182, doi: 10.1016/j.epsl.2009.12.019.

Naranjo, J.A., and Paskoff, R., 1985, Evolución cenozoica del piedemonte andino en la Pampa del Tamarugal, norte de Chile (18° -21°S): In IV Congreso Geologico Chileno, volume 4, pages 5–149 – 5–165. Universidad del Norte de Chile.

Nishiizumi, K., Caffee, M., Finkel, R., and Brimhall, G., 2005, Remnants of a fossil alluvial fan landscape of Miocene age in the Atacama Desert of northern Chile using cosmogenic nuclide exposure age dating. Earth and Planetary Science Letters, v. 237, 499-507, doi:10.1016/j.epsl.2005.05.032

Oncken, O., Chong, G., Franz, G., Giese, P., Gotze, H., Ramos, V., and Strecker, M., 2006, Deformation of the central andean plate system - Facts, fiction and constraints for plateau models, in The Andes - Active subduction orogeny, edited by Springer, pp.3-27, Berlin-Heidelberg

Rech, J., Currie, B., Michalski, G. and Cowan, A., 2006, Neogene climate change and uplift in the Atacama Desert, Chile, Geology, v.34(9), p. 761-764

Roering, J.J., Kirchner, J.W., and Dietrich, W.E., 1999, Evidence for non-linear, diffusive sediment transport on hillslopes and implications for landscape morphology, Water Resources Research, v.35, p.853-870

Schildgen, T., Hodges, K., Whipple, K., Reiners, P., and Pringle, M., 2007, Uplift of the western margin of the Andean plateau revealed from canyon incision history, southern Peru: Geology, v. 35, p. 523-526, doi: 10.1130/G23532A.1.

Schildgen, T. F., K. V. Hodges, K. X. Whipple, M. S. Pringle, M. C. van Soest, and K. Cornell, 2009, Late Cenozoic structural and tectonic development of the western margin of the central Andean Plateau in southwest Peru, Tectonics, 28, TC4007, doi: 10.1029/2008TC002403.

Schildgen, T. F., G. Balco, and D. L. Shuster, 2010, Canyon incision and knickpoint propagation recorded by apatite 4He/3He thermochronometry, Earth and Planetary Science Letters, 293(3-4), 377-387, doi: 10.1016/j.epsl.2010.03.009.

Schlunegger, F., Zeilinger, G., Kounov, A., Kober, F., and Husser, B., 2006, Scale of relief growth in the forearc of the Andes of Northern Chile (Arica latitude, 18°S): Terra Nova, v. 18, p. 217–223, doi: 10.1111/ter.2006.18.issue-3.

Schlunegger, F., F. Kober, G. Zeilinger, and R. von Rotz, 2010, Sedimentology-based reconstructions of paleoclimate changes in the Central Andes in response to the uplift of the Andes, Arica region between 19 and 21°S latitude, northern Chile, International Journal of Earth Sciences, 99(Supplement 1), 123-137, doi: 10.1007/s00531-010-0572-8.

Sillitoe, R. H., and E. H. McKee, 1996, Age of supergene oxidation and enrichment in the Chilean porphyry copper province, Economic Geology and the Bulletin of the Society of Economic Geologists, 91(1), 164-179.

Stock, J.D., and Montgomery, D.R., 1999, Geologic constraints on bedrock river incision using the stream power law: Journal of Geophysical Research, v. 104, p. 4983–4993, doi: 10.1029/98JB02139.

Strecker, M., Alonso, R., Bookhagen, B., and Carrapa, B., 2007, Tectonics and Climate of the Southern Central Andes: Annual Reviews Earth Planet. Sci, v. 35, p. 747–787, doi: 10.1146/annurev.earth.35.031306.140158.

Thouret, J.-C., G. Wörner, Y. Gunnell, B. Singer, X. Zhang, and T. Souriot, 2007, Geochronologic and stratigraphic constraints on canyon incision and Miocene uplift of the Central Andes in Peru, Earth and Planetary Science Letters, 263(3–4), 151–166, doi: 10.1016/j.epsl.2007.07.023.

Tucker, G.E., and Bras, R.L., 2000, A stochastic approach to modeling the role of rainfall variability in drainage basin evolution, Water Resources Research, 36(7): 1953-1964

Tucker, G.E., and Slingerland, R.L., 1994, Erosional dynamics, flexural isostasy, and long-lived escarpments: a numerical modeling study, Journal of Geophysical Research, 99: 12 229-12 243

556 Uba, C.E., Strecker, M.R., and Schmitt, A.K., 2007, Increased sediment accumulation rates and
557 climatic forcing in the central Andes during the late Miocene: Geology, v. 35, p. 979-982, doi:
558 10.1130/G224025A.1.

559 Victor, P., Oncken, O., and Glodny, J., 2004, Uplift of the western Altiplano plateau: Evidence from
560 the Precordillera between 20° and 21°S (northern Chile): Tectonics, v. 23, p. Tc4004, doi:
561 10.1029/2003TC001519.

562 Von Rotz, R., Schlunegger, F., Heller, F., and Villa, I., 2005, Assessing the age of relief growth in
563 the Andes of northern Chile: Magneto-polarity chronologies from Neogene continental sections:
564 Terra Nova, v. 17, p. 462–471, doi: 10.1111/j.1365-3121.2005.00634.x.

565 Whittaker, A.C., 2012, How do landscapes record tectonics and climate?: Lithosphere, v. 4, p. 160–
566 164, doi: 10.1130/RF.L003.1.

567 Willgoose, G.R., Bras, R.L., Rodriguez-Iturbe, I., 1991a, A physically based coupled network
568 growth and hillslope evolution model: 1 Theory, Water Resources Research, 27(7):1671-1684

569 Zeilinger, G., Schlunegger, F., and Simpson, G., 2005, The Oxaya anticline (northern Chile): a
570 buckle enhanced by river incision ?, Terra Nova, vol. 17, p. 368-375, doi: 10.1111/j.1365-
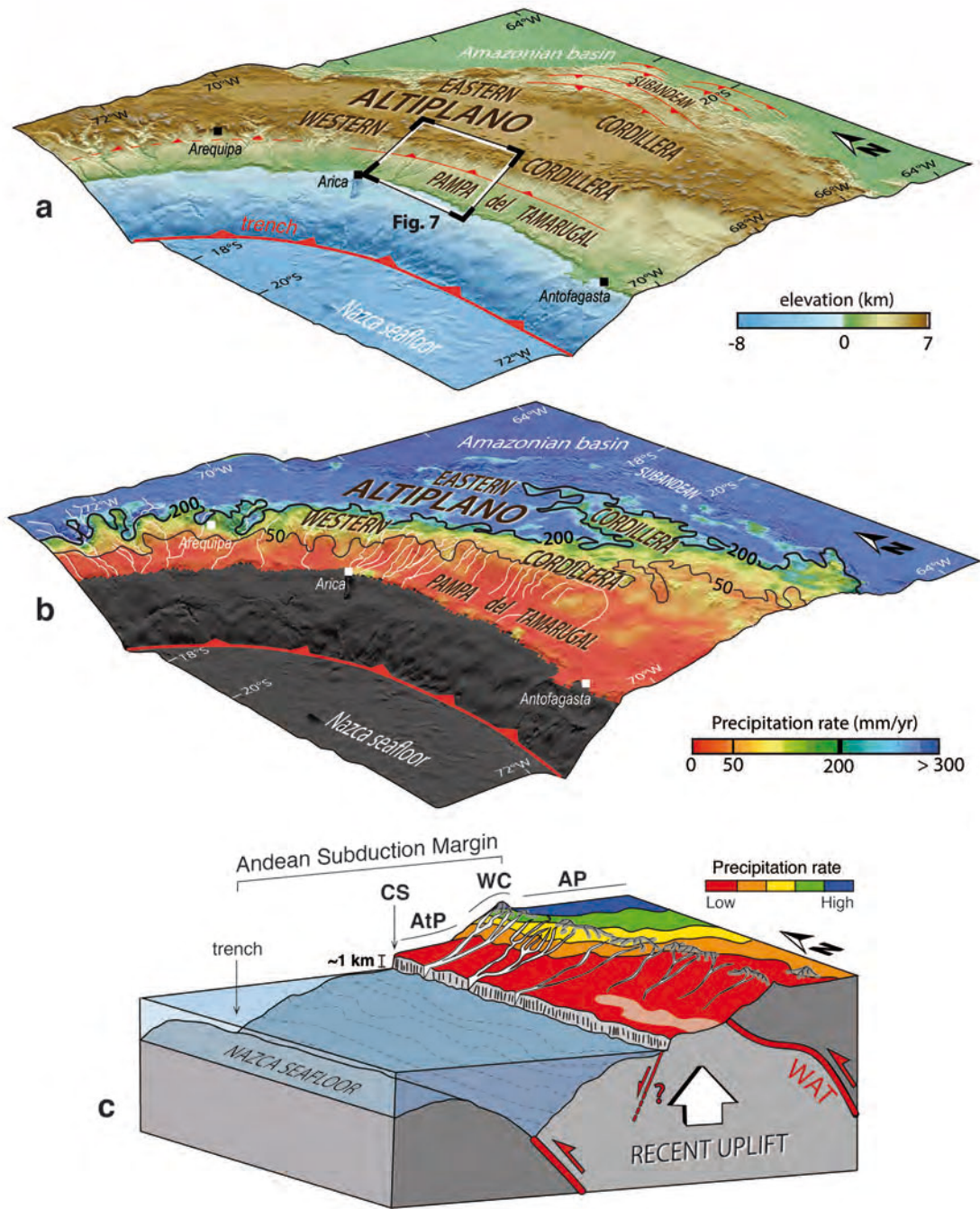571 3121.2005.00622.x

572

FIG.1: Topography and climate of the Central Andes. a/ 3D view from SW (vertical exaggeration of 10, SRTM30+ data) displaying main Andean units. The subduction zone (trench) and frontal thrusts of Western and Eastern Cordilleras are in red. White box outlines the threshold area where drainage morphology is analyzed in detail on Fig.8 and which correspond to 3D sketch below. b/ Topography overlaid with present-day mean precipitation rates derived from TRMM data (see also Fig.6). 50 and 200 mm/yr isohyets (precipitation isolines), in black, are oblique on bulk topography. The western hyper-arid region (<50 mm/yr) is in reddish colors. Precipitations on river headwaters are ≥200 mm/yr to the North and decrease to less than 50 mm/yr southward. c/ Cartoon of the threshold area illustrating tectonic and geomorphic processes: uniform recent uplift of the coastal Andean piedmont driven by recent faulting along the Coastal Scarp (CS), formation of endoreic drainage where rainfall is low and of canyons grading to the ocean where it is higher. AP, WC, WAT, AtP, are Western Cordillera, Altiplano, West Andean Thrust, Atacama Pediplain, respectively.
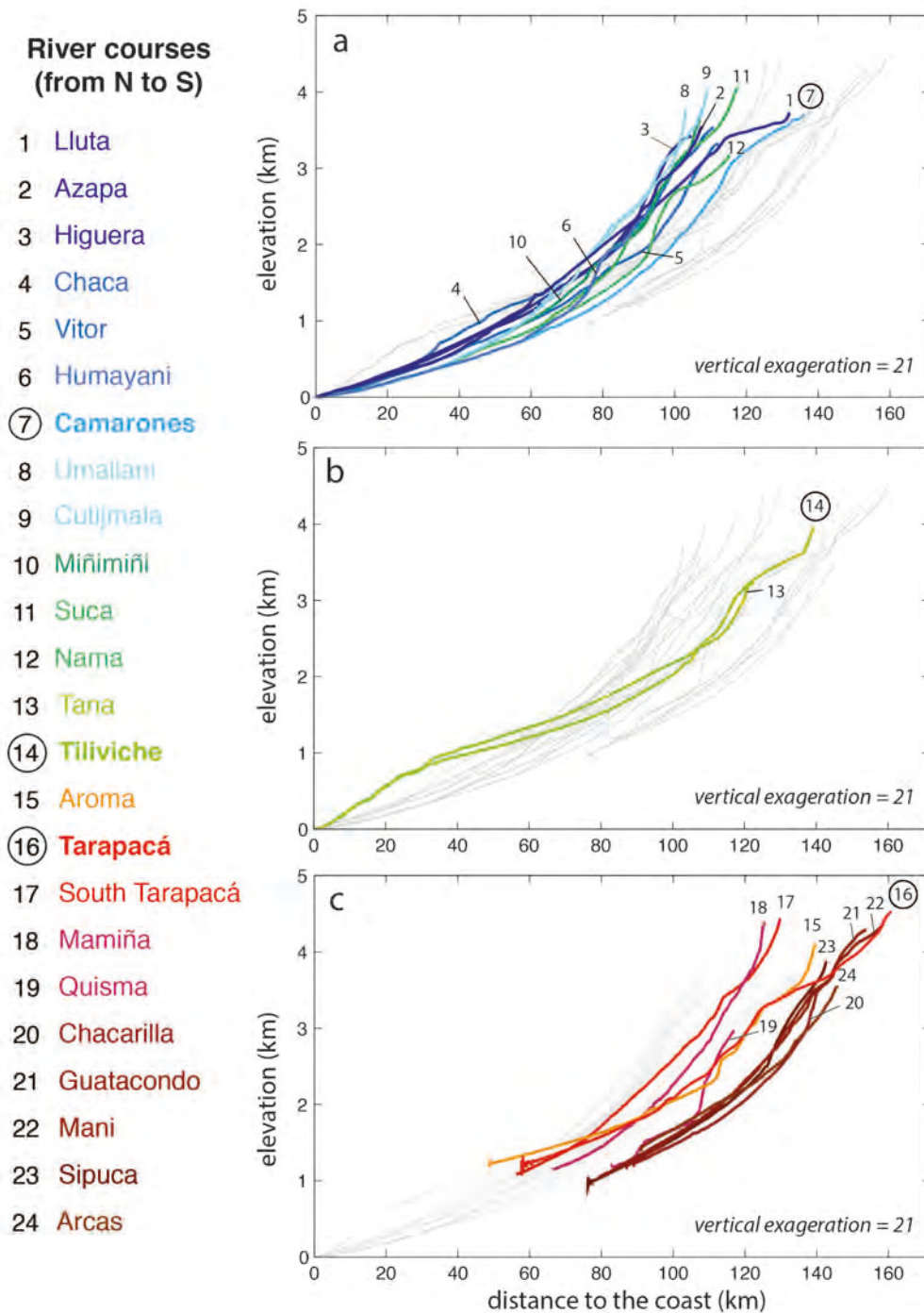
FIG.2: North Chile Topography (SRTM data) and geometry of the drainage network. Profiles of the main river channels, outlined in color, are analyzed in Fig.3 using the same color code (blue to red) and numbering increasing southward (1 to 24). The heavy dashed line indicates the main drainage divide on top of the Western Cordillera at the western border of the Altiplano. Thin dashed lines mark secondary minor streams (dry most of the time). The threshold between exoreic (to the North) and endoreic (to the South) drainage corresponds to rivers 13 and 14 (Tana - Tiliviche canyons) that present a prominent knick-point at ~25 km to the coast. The only river that crosses the Pampa del Tamarugal and Coastal Cordillera South of the threshold is the Loa river whose catchment area extends far more to the east than the others. View points a and b locate satellite and aerial views shown on Fig.4. Boxed area corresponds to area covered by the map of Fig.8a.

FIG.3: Longitudinal profiles of North Chile main river channels (shown with same colors than on the map of Fig.2) extracted from ASTER GDEM data (30 m horizontal resolution and <20 m vertical accuracy). A smoothing with a moving window (window width and overlap: 1 km and 0.4 km) and a wavelet fit are applied to remove spikes and anomalous values. The profiles are separated into three groups: **a/** Streams 1 to 12 with an overall concave up shape from high elevations (> 4 km a.s.l.) down to sea level; linked to the Pacific Ocean base-level. **b/** At the threshold, streams 13 and 14 have a convex upward lower course with a broad knickpoint from 0 to ~1 km a.s.l.. They remain linked to the ocean base-level. **c/** South of the threshold, rivers 15 to 24 vanish in the Pampa del Tamarugal at ~1 km a.s.l. Upper courses of rivers 13 to 24 have an overall concave shape from 4.5 down to 1 km a.s.l., marked by secondary knick-points due to recent uplift of the Western Cordillera (Hoke *et al.*, 2007).
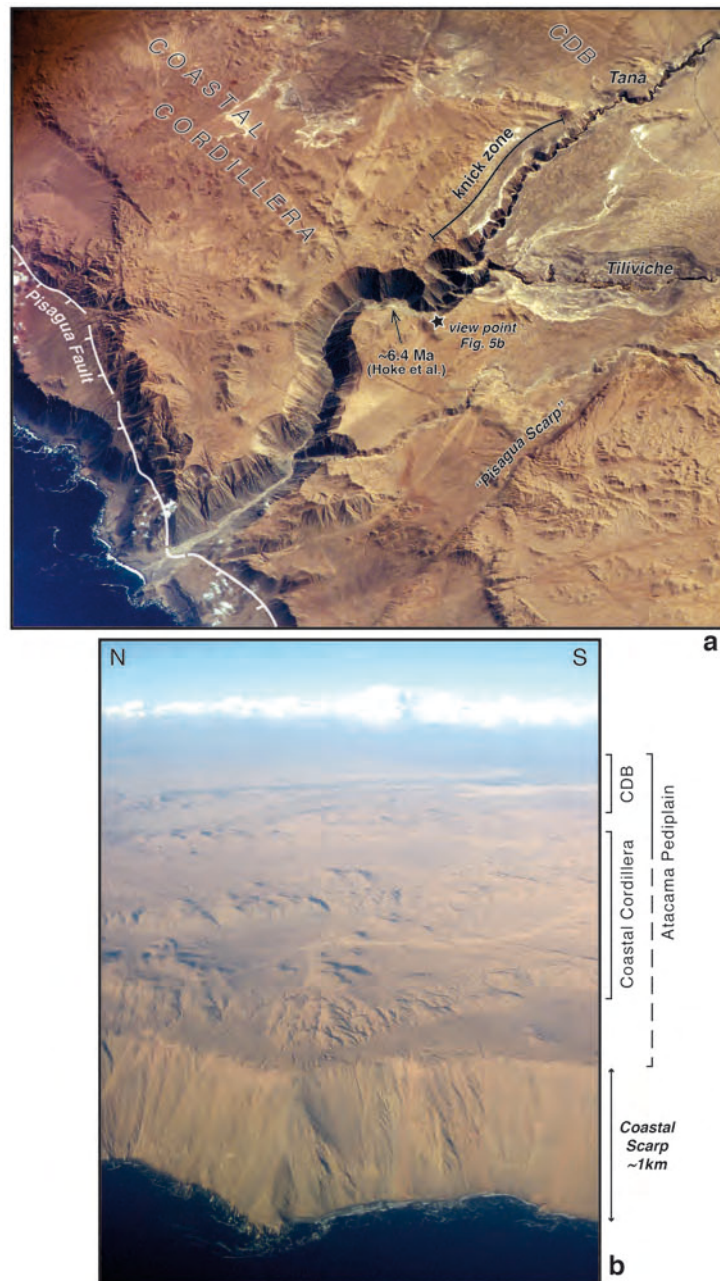
FIG.4: Satellite (**a**) and aerial (**b**) views of coastal morphology in the threshold area. **a/** Top satellite image (oblique view to NW taken from ISS, courtesy of NASA) shows outlet of Tana-Tiliviche canyon. The tenuously incised Tana upper channel becomes deeply incised downward across the knick zone located at ~25 km from the coast. The normal Pisagua Fault is parallel to the coastal scarp while the minor reverse "Pisagua scarp" (Almendinger *et al*., 2005) strikes ENE-WSW. Most of the incision post-date the terrace dated at ~6.4 Ma by [Hoke *et al*., 2007]. Note that the surface of the Atacama Pediplain and sediments linked to the Central Depression Basin (CDB) extend on both side of the canyon up to the Coastal Scarp (where they are offset by the Pisagua Fault), which suggests that the base-level was already set by the ocean before the onset of tectonically-driven uplift and correlative canyon incision. The star locates the viewpoint of panorama from Fig.5b. **b/** Bottom aerial view (courtesy A. Bonacin) shows the impressive Coastal Scarp ~35 km south of Tana-Tiliviche outlet with the Atacama pediplain and the subdued relief of the Coastal Cordillera perched on top. CDB marks location of the Central Depression Basin in the background.
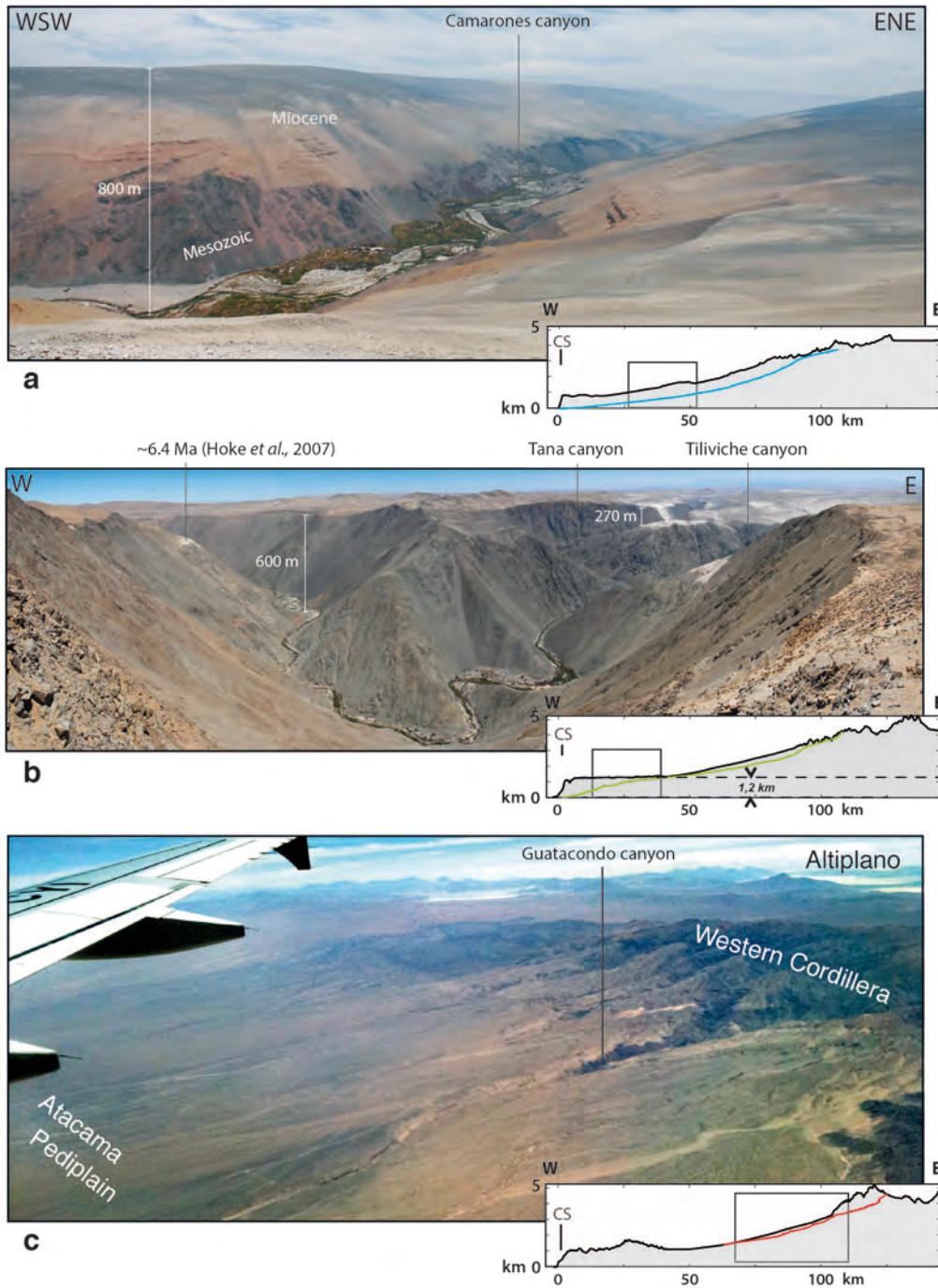
FIG.5: Field views of typical North Chile river morphologies. Lower right insets show the selected river profiles (Camarones, Tiliviche, Tarapacá, Figs. 2, 3, 8) and surrounding topography (box shows part of the profile displayed by the photograph). **a/** The Camarones canyon, north of the geomorphic threshold, is incised more than 800 m below the Atacama Pediplain surface within Miocene sediments of the Central Depression Basin and its Mesozoic basement. **b/** Panoramic view of the main knick-point characterizing the geomorphic threshold (Tana - Tiliviche canyons). The streams, little incised in the background (right), become deeply entrenched downward into the Mesozoic basement (left). **c/** Aerial view (courtesy Y. Lagabrielle) of river channels south of the threshold. The Guatacondo river, in the foreground, which incises the W Cordillera flank and aggrades on the Atacama Pediplain, is similar to the Tarapacá canyon (located more to the North) whose profile is shown on the lower right and on Fig.8.
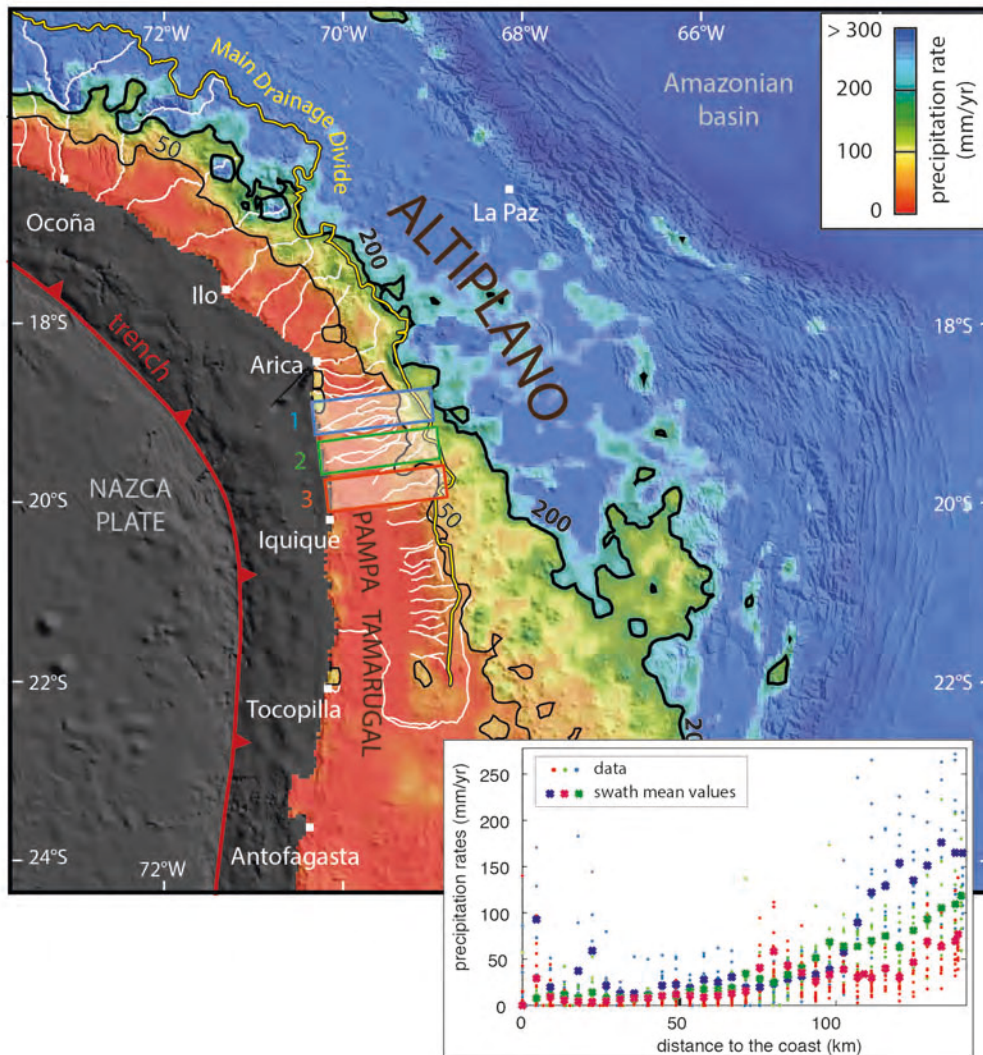
FIG.6: Present-day climatic pattern of the southern Central Andes. Rainfall data (mean annual precipitation rates) come from the TRMM 2B31 dataset, (Bookhagen & Strecker, 2008) covering a 9-years long period (1998-2006) and calibrated from field measurements at rain gauge stations. TRMM (Tropical Rainfall Measurement Mission, joint mission of NASA and JAXA) data are available from http://trmm.gsfc.nasa.gov/ and TRMM 2B31 dataset from B. Bookhagen web page: http://www.geog.ucsb.edu/~bodo/TRMM/index.php. We applied a smoothing to original data (0.04° horizontal resolution) using a 5*5 pixel kernel. The color scale is chosen to enhance visualization of driest areas (less than 300 mm/yr). Thin and heavy black lines indicate the 50 mm/yr and 200 mm/yr isohyets, respectively. These isohyets are oblique to the topography of the Altiplano plateau. River (in white) catchment areas reach the 200 mm/yr curve to the NW and become restricted southward below the 50 mm/yr isohyet (except for the Loa river). Boxes numbered 1 to 3 correspond to the three swath profiles shown on the graph below: blue (box 1, North of threshold), green (box 2, threshold) and red (box 3, South of threshold).
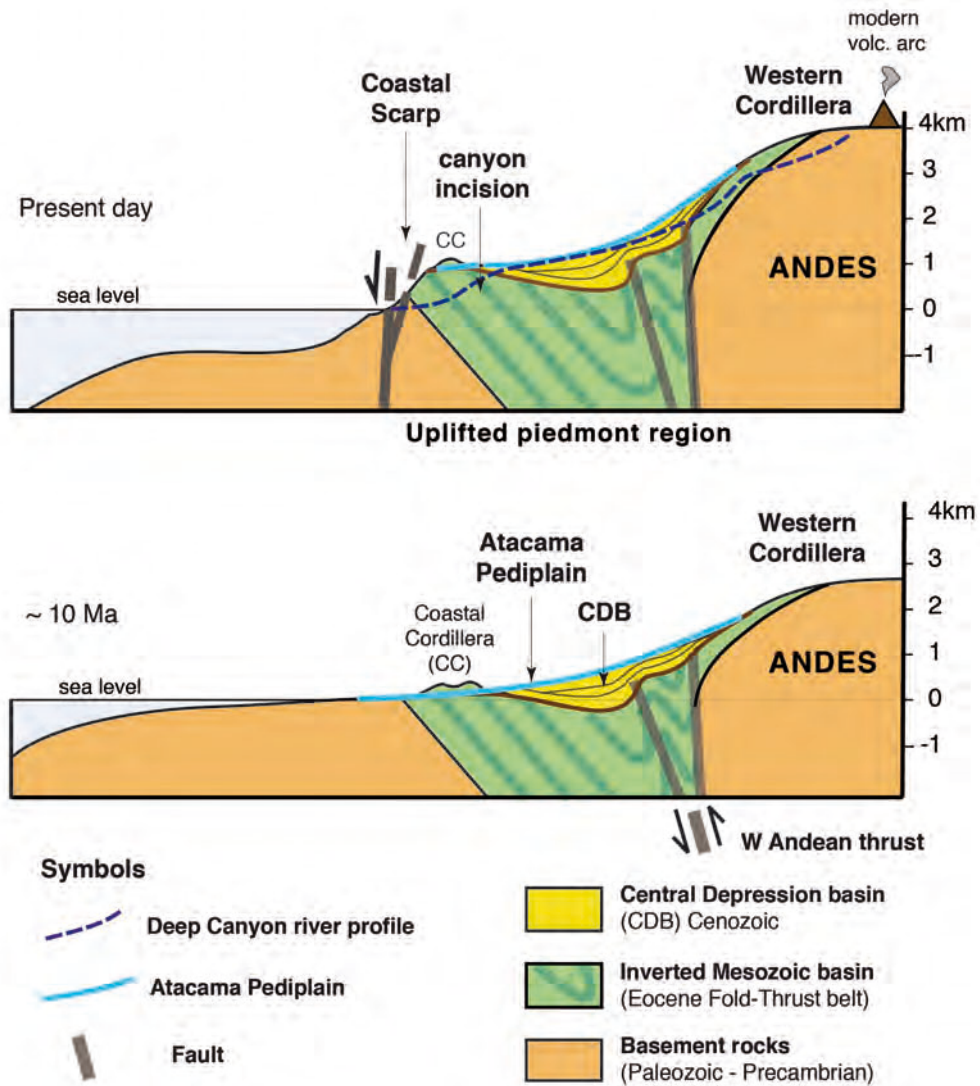
FIG.7: Schematic morpho-tectonic evolution of the west Andean margin for the last 10 My. (Top) Present-day topography and geology of the coastal topography. The Atacama Pediplain (AtP) is hanging at 1 km a.s.l. and is interrupted towards the coast by the giant Coastal Scarp. The AtP corresponds to the top surface of a continental wedge-shaped basin: the Central Depression Basin, which is deeply incised by rivers all the way from the Western Cordillera to the ocean. (Bottom) Possible reconstruction of the 10 Ma topography of the west Andean margin. The Atacama Pediplain is a smooth and continuous surface that connects with the ocean base level.
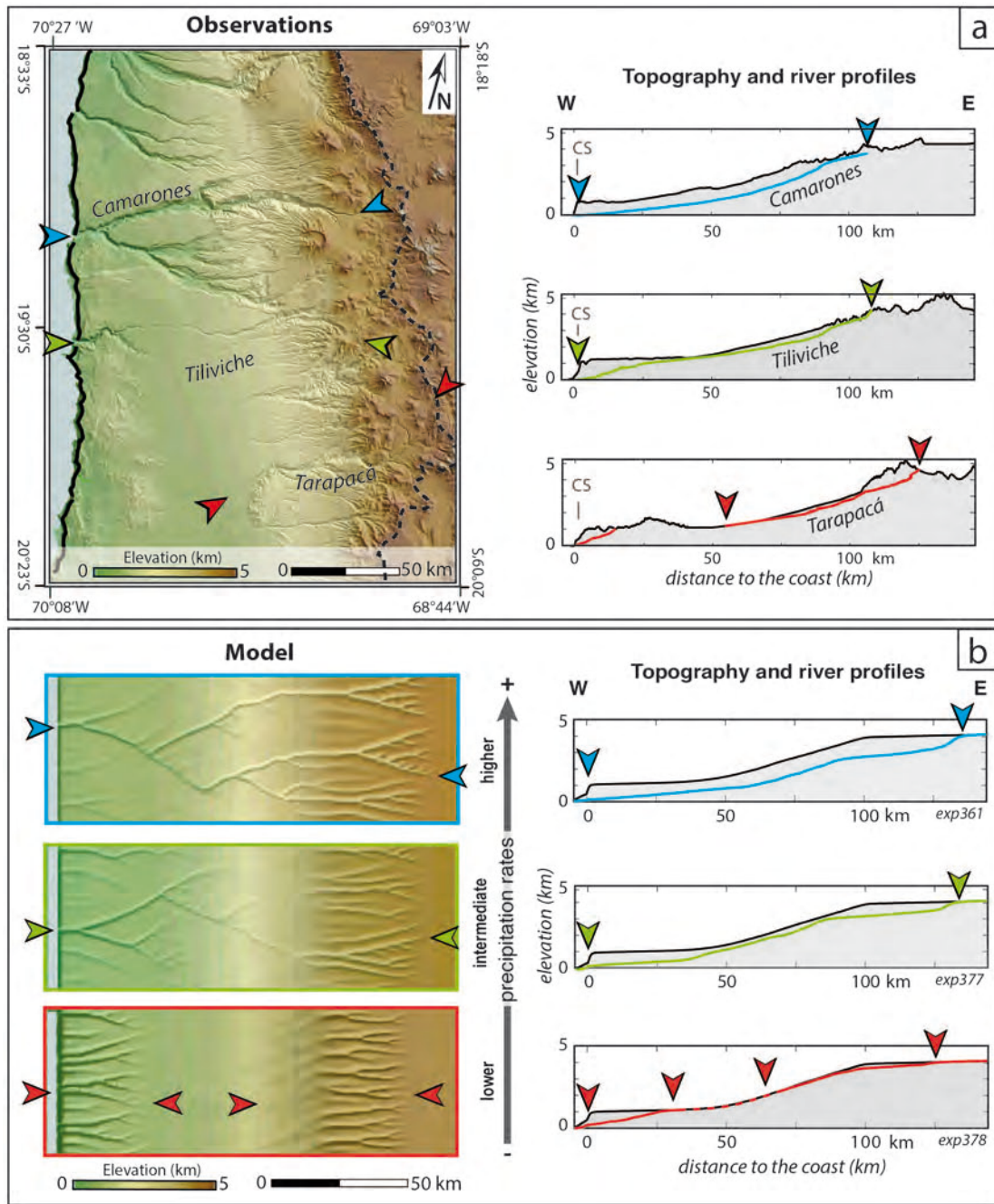
FIG.8: Geomorphology of the threshold area (see location on Fig.1 and 2). **a/** Map view (left) displays the three channels selected to illustrate the threshold between exoreic and endoreic drainage. On the right: longitudinal river profiles (projected E-W) and surrounding topographic envelope for these three typical valleys: Camarones (North of threshold, linked to ocean base-level and deeply entrenched), Tiliviche (threshold, convex upward and with prominent knick-point), Tarapacá (South of threshold, endoreic). **b/** Selected modeling results (map views) for three different mean precipitation rates (see Fig.S5 for a view of the whole experimental boxes). Same initial topography and uplift rates are used for all the experiments. On the right, representative topography and river profiles, drawn for the streams outlined by arrows on map views to the left, to be compared with Camarones, Tiliviche and Tarapacá river profiles.